Cell, Vol. 105, 269–279, April 20, 2001, Copyright ©2001 by Cell Press

Crystal Structure of a SIR2 Homolog–NAD Complex

Jinrong Min,* Joseph Landry,† Rolf Sternglanz,† and Rui-Ming Xu*‡
*W. M. Keck Structural Biology Laboratory
Cold Spring Harbor Laboratory
Cold Spring Harbor, New York 11724
†Department of Biochemistry and Cell Biology
State University of New York, Stony Brook
Stony Brook, New York 11794

Summary

The SIR2 protein family comprises a novel class of nicotinamide-adenine dinucleotide (NAD)-dependent protein deacetylases that function in transcriptional silencing, DNA repair, and life-span extension in *Saccharomyces cerevisiae*. Two crystal structures of a SIR2 homolog from *Archaeoglobus fulgidus* complexed with NAD have been determined at 2.1 Å and 2.4 Å resolutions. The structures reveal that the protein consists of a large domain having a Rossmann fold and a small domain containing a three-stranded zinc ribbon motif. NAD is bound in a pocket between the two domains. A distinct mode of NAD binding and an unusual configuration of the zinc ribbon motif are observed. The structures also provide important insights into the catalytic mechanism of NAD-dependent protein deacetylation by this family of enzymes.

Introduction

Genes located in certain regions of eukaryotic chromosomes are permanently repressed. This heritable, transcriptionally silent state is caused by an altered chromatin structure that can be propagated from one generation to the next. This phenomenon of epigenetic control of gene expression has been observed in organisms ranging from yeast to human. Examples of transcriptional silencing include mating-type loci in fission and budding yeasts, position effect variegation in *Drosophila*, and X chromosome inactivation in mammals (reviewed in Laurenson and Rine, 1992; Weiler and Wakimoto, 1995; Allshire, 1996; Lyon, 1999). In *S. cerevisiae*, silencing is observed for at least three genomic loci: the silent mating-type loci, *HML* and *HMR* (Rine and Herskowitz, 1987), telomeres (Gottschling et al., 1990; Aparicio et al., 1991), and the ribosomal DNA region (Bryk et al., 1997; Fritze et al., 1997; Smith and Boeke, 1997). A set of proteins, the silent information regulators (SIR), SIR1, SIR2, SIR3, and SIR4 are important for the establishment and maintenance of gene silencing (reviewed in Loo and Rine, 1995). In mating-type and telomeric silencing, SIR2, SIR3, and SIR4 form a multiprotein complex that binds to the nucleosome (Moretti et al., 1994; Hecht et al., 1995, 1996; Moazed et al., 1997; Strahl-Bolsinger et al., 1997). A different SIR2-containing protein complex is responsible for rDNA silencing (Shou et al., 1999; Straight et al., 1999). The SIR protein complex interacts with the N-terminal tails of histones H3 and H4, and this interaction is thought to be responsible for chromatin silencing (Johnson et al., 1990; Hecht et al., 1995).

In addition to their silencing function, SIR proteins also mediate repair of chromosomal double-strand breaks through nonhomologous end-joining (Tsukamoto et al., 1997; reviewed in Gartenberg, 2000). SIR2 has also been implicated in promoting longevity in yeast mother cells (reviewed in Guarente, 2000). The function of SIR2 in aging appears to be linked to its role in suppressing rDNA recombination. It is believed that accumulation of extrachromosomal rDNA circles formed during rDNA recombination is a major cause of aging. SIR2 functions in aging by suppressing rDNA circle formation.

SIR2 is unique among the SIR proteins (reviewed in Gottschling, 2000). It is the only protein required for silencing in all three silent loci studied, and it is the only one that has been evolutionarily conserved in diverse organisms ranging from bacteria to human (Brachmann et al., 1995; Afshar and Murnane, 1999; Frye, 1999; Sherman et al., 1999; see Figure 1A). The precise function of the SIR2 family of proteins was not known until recently. Inspired by earlier observations that the SIR2-like proteins are phosphoribosyltransferases (Tsang and Escalante-Semerena, 1998; Frye, 1999; Tanny et al., 1999), several groups reported that this family of proteins exhibits NAD-requiring histone deacetylase activity in vitro (Imai et al., 2000; Landry et al., 2000a; Smith et al., 2000). The discovery of histone deacetylase activity of the SIR2 family of proteins is particularly enlightening in the context of silencing because it has been previously reported that silencing is associated with reduced acetylation (Braunstein et al., 1993). SIR2 mutants defective in in vitro deacetylase activity also derepress silenced genes and have a reduced life span, suggesting that deacetylase activity is essential for the function of SIR2 in vivo. Furthermore, null mutants of *NPT1*, a gene that functions in NAD synthesis, show phenotypes similar to that of *sir2* mutants in silencing (Smith et al., 2000) and in life-span extension in response to caloric restriction (Lin et al., 2000). Taken together, these results strongly argue that the NAD-dependent protein deacetylase activity is critical for the physiological function of SIR2.

There are multiple SIR2 homologs in eukaryotes. Some of them have been implicated in silencing, as well as in proper cell cycle progression, radiation resistance, and genomic stability (Brachmann et al., 1995). Bacterial, archaeal, and many of the other SIR2 homologs are less well characterized than yeast SIR2 (Sherman et al., 1999; Cockell et al., 2000; Cuperus et al., 2000), and their physiological functions are not presently clear. Nevertheless, all SIR2 homologs tested to date share NAD-dependent deacetylase activity (Imai et al., 2000; Landry et al., 2000a; Smith et al., 2000), strongly suggesting that the enzymatic activity is key to the function of the SIR2 family of proteins. The enzymatic mechanism of the SIR2 family of deacetylases differs from previously

‡To whom correspondence should be addressed (e-mail: xur@cshl.org).

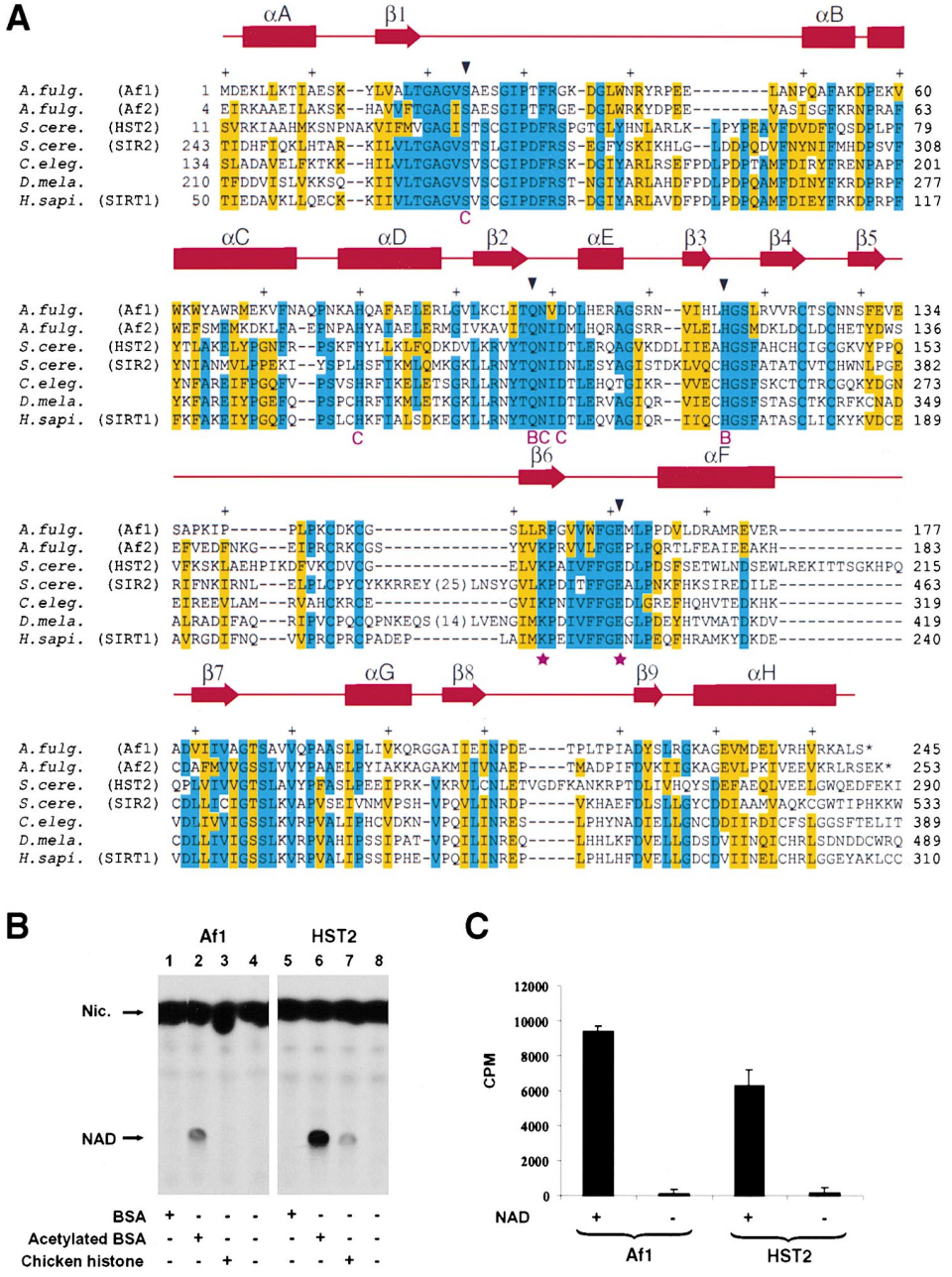

Figure 1. Sequence and Functional Conservation of SIR2-Af1

(A) Sequence alignment of SIR2 homologs. Positions at which five or more sequences are identical are highlighted cyan. Positions at which five or more are similar are highlighted yellow. Accession numbers of the sequences are 7448869 (Af1), 7448871 (Af2), 6320163 (SIR2), 1708326 (HST2), 7298007 (*D. melanogaster*), 7506617 (*C. elegans*), and 9884660 (human SIRT1). The positions of α helices and β strands are indicated above the sequence. Every 10 residues of SIR2-Af1 is indicated with a + sign above the sequence. An arrowhead above the sequence indicates the positions where HST2 residues have been mutated (results shown in Figure 5). A star below the sequence indicates residues involved in the R153:E161 salt bridge. Magenta letters, B and C, below the sequence, indicate the location of these residues in the B and C sites of the NAD binding pocket as defined in Figure 3C.

(B) NAD-nicotinamide exchange activity of SIR2-Af1. Reactions were performed in the presence of BSA (lane 1), acetylated BSA (lane 2), chicken histones (lane 3), and buffer alone (lane 4). Lanes 5–8 show the results with HST2 protein. The positions of nicotinamide and NAD are indicated.

(C) NAD-dependent deacetylase activity of SIR2-Af1 and yeast HST2 as measured by the release of [^{3}H]acetate (see Experimental Procedures) from ^{3}H-labeled acetylated BSA. Activity is expressed as the cpm remaining after subtracting the value obtained for a minus enzyme plus NAD control.

characterized histone deacetylases. Deacetylation of acetyl-lysine is tightly coupled to NAD hydrolysis, producing a novel acetyl-ADP ribose compound (1-O-acetyl-ADP ribose) (Landry et al., 2000b; Tanner et al., 2000; Tanny and Moazed, 2001). To understand the structural basis of the enzymatic mechanism of the SIR2 protein family, we report here the crystal structure of a SIR2 homolog from *Archaeoglobus fulgidus*, SIR2-Af1, complexed with NAD. Structures from two different crystal forms were solved, one at 2.1 Å and the other at 2.4 Å resolution. Because of evolutionary conservation in sequence and in enzymatic function, the structure of the archaeal enzyme should provide a basis for the further understanding of the structure and function of the SIR2 family of proteins.

Results

Overview

The genome of *Archaeoglobus fulgidus* encodes two ORFs, termed SIR2-Af1 and SIR2-Af2 here, that are similar to yeast SIR2. The two proteins share 47% sequence identity with each other, and they share 24% and 27% sequence identity with SIR2, respectively (Figure 1A). Purified SIR2-Af2 has previously been shown to have NAD-dependent histone deacetylase activity in vitro (Smith et al., 2000). We show here that SIR2-Af1 is also a NAD-dependent protein deacetylase. First, SIR2-Af1 catalyzes nicotinamide-NAD exchange (Figure 1B) (Landry et al., 2000a). Second, SIR2-Af1 deacetylates ^{3}H-labeled BSA in a NAD-dependent manner (Figure 1C). Interestingly, SIR2-Af1 displays protein substrate specificity different from other SIR2-like proteins tested (Imai et al., 2000; Landry et al., 2000a; Smith et al., 2000), in that it does not deacetylate eukaryotic histones in vitro and histones do not stimulate nicotinamide-NAD exchange (Figure 1B). Synthetic histone H3 and H4 peptides acetylated at various lysine residues also do not stimulate the nicotinamide-NAD exchange activity of SIR2-Af1 (data not shown). It is worth noting that archaea lack eukaryotic-like histone N-terminal tails. Nevertheless, SIR2-Af1 displays robust nicotinamide-NAD exchange and NAD-dependent protein deacetylase activities toward a general substrate, acetylated BSA (Figures 1B and 1C). These results confirm that SIR2-Af1 is a member of the SIR2 family of NAD-dependent protein deacetylases.

The SIR2-Af1/NAD complex crystallized in two crystal forms, one in an orthorhombic spacegroup $C222_1$ and the other in a monoclinic C2 spacegroup. The orthorhombic crystal structure of SIR2-Af1/NAD was determined by the method of multiwavelength anomalous diffraction (MAD) to 2.4 Å resolution using mercury as an anomalous scatterer (Figures 2A and 2B). The monoclinic crystal structure was solved by molecular replacement to 2.1 Å resolution using the orthorhombic structure as a search model. Phasing and refinement statistics are shown in Table 1. There are two protein/NAD complexes per asymmetric unit in both crystal forms. The dimers appear to be nonphysiological, because protein contacts in the asymmetric unit are different in the two crystal forms and they involve nonconserved amino acids and solvent molecules. Dynamic light scattering in solution also shows that SIR2-Af1 exists as a monomer (data not shown). The apparent monomeric state of SIR2-Af1 differs from that of SIR2, which appears to interact with itself, forming a multimer in vitro (Moazed et al., 1997). The two molecules in the asymmetric unit have similar conformations in both crystal forms. The root-mean-squared (rms) deviations between the two molecules in each crystal form were 0.59 Å for the monoclinic form and 0.60 Å for the orthorhombic form. Henceforth, the structure of one SIR2-Af1/NAD complex from each crystal form will be described.

The overall folding of SIR2-Af1 is similar in both crystal forms and the 2.1 Å monoclinic structure is shown as a ribbon model in Figure 2C. The protein consists of eight α helices (αA–αH) and nine β strands (β1–β9) organized in two domains. The large domain has a classical open α/β, Rossmann-fold structure (Figure 2D). Six parallel strands (β1–β3 and β7–β9) form a central β sheet which is sandwiched between four α helices (αA, αD, αE, and αH) on one side (back) of the β sheet and two (αF and αG) on the other side (front). The small domain consists of a three-stranded antiparallel β sheet (β4–β6), two α helices (αB and αC), and a large portion of the long loop connecting β1 and αB (L-1B; loops are designated by their flanking secondary structures). A zinc ion in the native protein crystal (a mercury ion in the orthorhombic structure) is bound by two pairs of cysteines (Cys124 and Cys127, and Cys145 and Cys 148) located near the tip of β4-turn-β5 and on the loop immediately N-terminal to β6, respectively. The three-stranded four-cysteine metal binding site resembles the Zn-ribbon structure of transcription factors TFIIS (Qian et al., 1993), TFIIB (Zhu et al., 1996), and the RNA polymerase II subunit RPB9 (Wang et al., 1998). Interestingly, a conserved salt bridge involving the pairing of Arg153 and Glu161 is found to contribute to the positioning of the Zinc-ribbon motif with respect to the rest of the structure (Arg153 is located in β6 of the small domain, and Glu153 is in the middle of loop L-6F connecting the two domains) (Figure 2C). The two domains are clearly defined, even though they are in close contact. One NAD molecule is bound in a pocket between the two domains, directly above the crevice formed at the topological switch point of the large domain, and below loop L-1B.

The most significant difference between the monoclinic and the orthorhombic structures occurs at an 18 amino acids segment (Pro30–Leu47) of loop L-1B. In Figure 2C, the loop segment from the 2.4 Å orthorhombic structure (shown in magenta) is superimposed onto the 2.1 Å monoclinic structure (its loops are shown in orange). The rms deviations for Cα atoms between the two structures are 2.3 Å (the loop segment excluded in superposition) or 8.4 Å (all Cα atoms included). In both structures, the loop segment forms a flap above the NAD binding pocket. The monoclinic crystal structure represents a form with a more accessible NAD binding pocket (open state) and the orthorhombic structure shows a reduced accessibility of the binding pocket (closed state). This loop segment is likely to be dynamic in solution, as both conformations were stabilized by protein–protein interactions: a crystallographic and a noncrystallographic protein–protein interaction in the monoclinic and the orthorhombic structure, respectively.

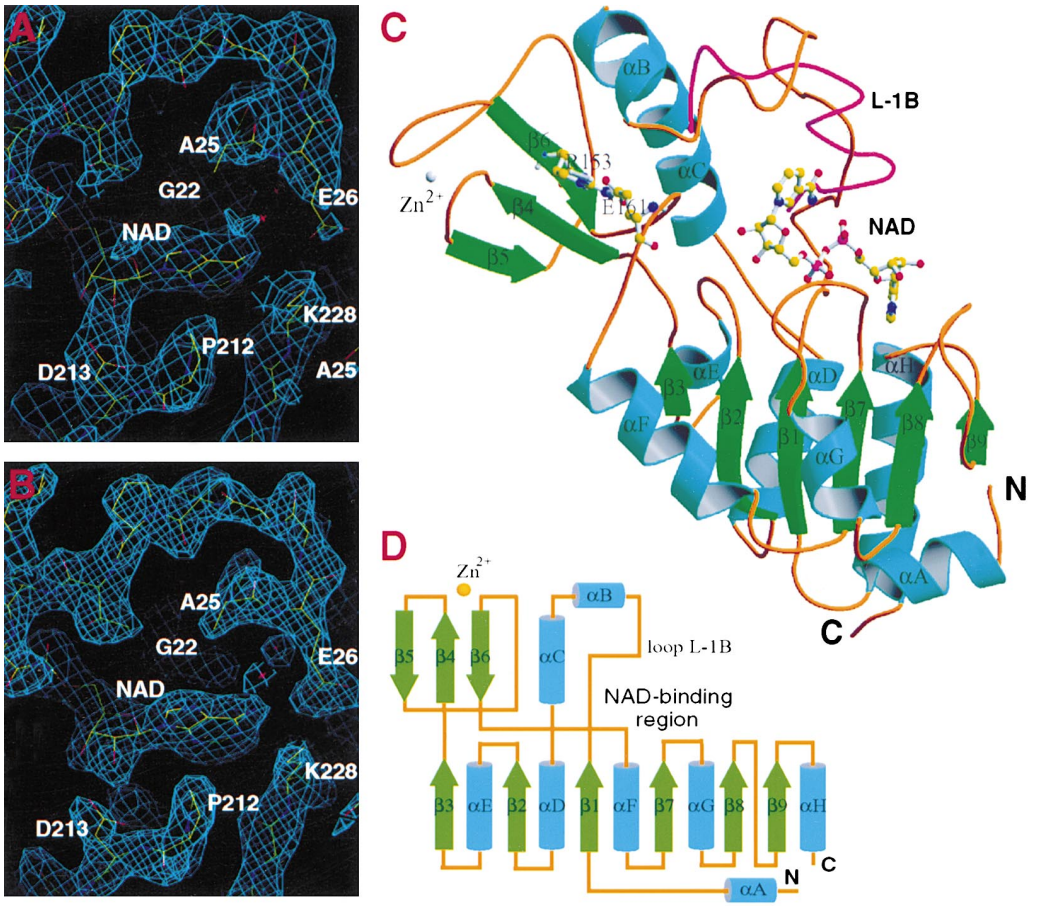

Figure 2. Overall Structure of SIR2-Af1

(A) The 2.8 Å resolution MAD-phased electron density map is shown around the adenine base. The map is contoured at 1σ level, and the refined 2.4 Å structure is superimposed.

(B) The 2.4 Å 2Fo-Fc map showing the same region as in (A). The map is contoured at 1.5 σ level.

(C) The 2.1 Å monoclinic structure is shown in a ribbon representation. The conformation of a loop L-1B segment from the 2.4 Å orthorhombic structure is significantly different, and it is superimposed and shown in magenta. A bound NAD molecule is shown in a ball-and-stick model (oxygen: red; carbon: yellow; nitrogen: blue; and phosphorus: magenta). A zinc ribbon motif is present in the small domain. The zinc ion is shown as a white ball. The R153:E161 salt bridge is also shown in a ball-and-stick model. Not shown in the figure is an eleven amino acid tag (including 6 consecutive histidines) fused at the N terminus of the protein. The tag is next to β9 and the loop connecting β8 and β9. The figure was generated by MOLSCRIPT (Kraulis, 1991) and Raster3D (Merritt and Bacon, 1997).

(D) Topological diagrams of secondary structure elements. NAD and zinc binding sites are indicated.

Protein–NAD Interaction

The NAD molecule adopts an extended conformation, which is commonly found when NAD is bound to a protein having a Rossmann fold. Significantly, the NAD molecule is oriented in an inverted direction compared with other NAD-linked dehydrogenases (Rossmann et al., 1975). The adenine base binds to the C-terminal half of the β sheet and the nicotinamide group binds to the N-terminal half (Figure 2C). Interestingly, a search for homologous structures using the Dali server (Holm and Sander, 1996) revealed that the closest structure (Z-score: 14.0; rms deviation of Cα atoms: 2.1 Å) is the NADP(H) transhydrogenase (TH) domain III (Prasad et al., 1999). The TH structure is the only other example we could find in which the NADP molecule is bound in an inverted direction. In the SIR2-Af1 structure, the adenine base is in an anti conformation with the ring perpendicular to the β sheet plane. The adenine ribose has a 2′-endo sugar puckering. The adenine ribose and the pyrophosphate moieties have nearly identical conformations in the two structures. The precise position of the nicotinamide group cannot be modeled in either structure due to weak electron densities. Nevertheless, the ribose connected to the nicotinamide group is ordered in both structures, and the general location of the nicotinamide can be inferred from the position of the ribose group. The ribose ring has a 3′-endo sugar puckering in the open state, and a 2′-endo sugar puckering in the closed conformation.

The NAD molecule is bound in an extensive pocket between the large and the small domains of the protein. The NAD binding pocket in the open conformation is shown in Figures 3A–3C. The large domain forms the "floor", and the small domain, loop L-1B in particular, forms the "ceiling" of the NAD binding pocket. Most of the conserved residues of the NAD binding pocket are located on the "floor", and they show few conformational differences between the two structures. The NAD

Table 1. Summary of Crystallographic Analysis

Data Sets	Native	λ0	λ1	λ2	λ3
Diffraction data					
Resolution (Å)	2.1	2.4	2.8	2.8	2.8
Measured reflections	85113	114619	34330	33107	41988
Unique reflections	30346	19977	12263	12079	12339
Completeness (%)	90.9	91.4	86.3	86.6	88.3
Average I/σ	13.1	19.4	22.5	18.3	19.2
R_{merge} (%)*	6.5	5.9	3.7	4.4	4.1
Phasing					
Phasing power† at 2.8 Å					
Anamalous/isomorphous			2.90/	3.39/0.83	3.38/0.96
Overall figure of merit			−0.57		
Refinement					
Resolution range (Å)	40.0–2.1	20.0–2.4			
Reflections used ($I/\sigma > 0$)	30208	19933			
R factor‡/R_{free} (%)	19.9/24.9	20.4/26.7			
Number of protein/NAD atoms	3898/88	3832/88			
Number of metal ions	2	2			
Number of water molecules	261	103			
Rms deviations					
bond lengths	0.009 Å	0.008			
bond angles	1.51°	1.38°			
dihedrals	22.8°	23.1°			
improper	1.17°	1.05°			

*$R_{merge} = \Sigma|I - \langle I\rangle|/\Sigma\langle I\rangle$, where I and $\langle I\rangle$ are the measured and averaged intensities of multiple measurements of the same reflection. The summation is over all observed reflections.
†Phasing power = rms. ($\langle F_H\rangle/E$), where F_H is the calculated structure factor of the heavy atoms and E is the residual lack of closure.
‡R factor = $\Sigma||F_O| - |F_C||/\Sigma|F_O|$, where F_O denotes the observed structure factor amplitude and F_C denotes the structure factor calculated from the model.

binding pocket can be divided into three regions (Figure 3C): (1) site A, where the adenine-ribose moiety of NAD is bound; (2) site B, where the nicotinamide-ribose moiety is bound; and (3) site C, which is deep inside the pocket and is not near the position of observed NAD. A schematic drawing showing protein–NAD interactions is shown in Figure 3D. Our mutagenesis data have implicated the involvement of sites B and C in the deacetylation and NAD hydrolysis reactions (see below).

The A site is a shallow, mostly hydrophobic and exposed pocket near the C-terminal ends of β7 and β8 (Figures 3B and 3C). The base is surrounded by amino acids Gly22, Ala25, Glu26, Gly185, Pro212, Lys228, and Ala229 (Figure 3D). Among these, Gly22 and Gly185 are perfectly conserved among all SIR2 family members. They are located at positions immediately C-terminal to β1 and β7, respectively, and are on the same side of the adenine base forming the inner wall of the A site. Glycines are conserved at these positions probably because they do not have side chains and would not introduce steric clashes with the adenine base. Ala25 and Glu26 are located on the same side of the base as the glycines. They form the rim of the A site and sequences for these positions are variable. The side chain of Glu26 makes a hydrogen bond with the N6 atom of the base. The nonconserved residues Pro212 and Lys228 are on the other side of the adenine base; they contact the base through van der Waals interactions. Ala229 is located in the back of the base, and the main chain amide makes a hydrogen bond with the N1 atom of the adenine ring. The 2′ hydroxyl group of the adenine ribose forms one hydrogen bond with Asn211 and one with Asp213. The 3′ hydroxyl makes another hydrogen bond with Asn211. Common to both crystal forms, the O2 atom of the α-phosphate makes a hydrogen bond with the hydroxyl group of Ser187, and the O1 atom of the β-phosphate makes hydrogen bonds with the main chain amide group of Thr186 and the side chains of Thr186 and Ser187. Conformational differences of loop L-1B in the two crystal forms introduce different interactions between the pyrophosphate moiety and the protein. Most notably, the O1 atom of the α-phosphate hydrogen bonds with the main chain amide of Phe32 and Arg33 in the orthorhombic structure, and a water mediated interaction between O1 and Arg33 is observed in the monoclinic structure.

The B site is the binding site for the nicotinamide ribose moiety. The "floor" at the B site is very similar between the two structures, but the "ceiling" has been "raised" in the monoclinic structure due to the conformational difference of loop L-1B. In the orthorhombic structure, the nicotinamide ribose is surrounded by conserved hydrophobic residues Phe32, Trp39, and Val190. All of the aromatic residues moved away from the nicotinamide ribose moiety, by as much as 13 Å in the case of Trp39, in the monoclinic crystal form. Many more water molecules are present near the nicotinamide ribose binding region in the "open" state of the NAD binding pocket in the monoclinic structure. The O3′ atom makes a hydrogen bond with His116, and it also interacts with the carbonyl group of Gln98 in both structures. Both Gln98 and His116 are located on the "floor" of the NAD binding pocket. The nicotinamide group is disordered in both structures, but its general location can be inferred from the position of the ordered ribose group. In the orthorhombic structure, the nicotinamide

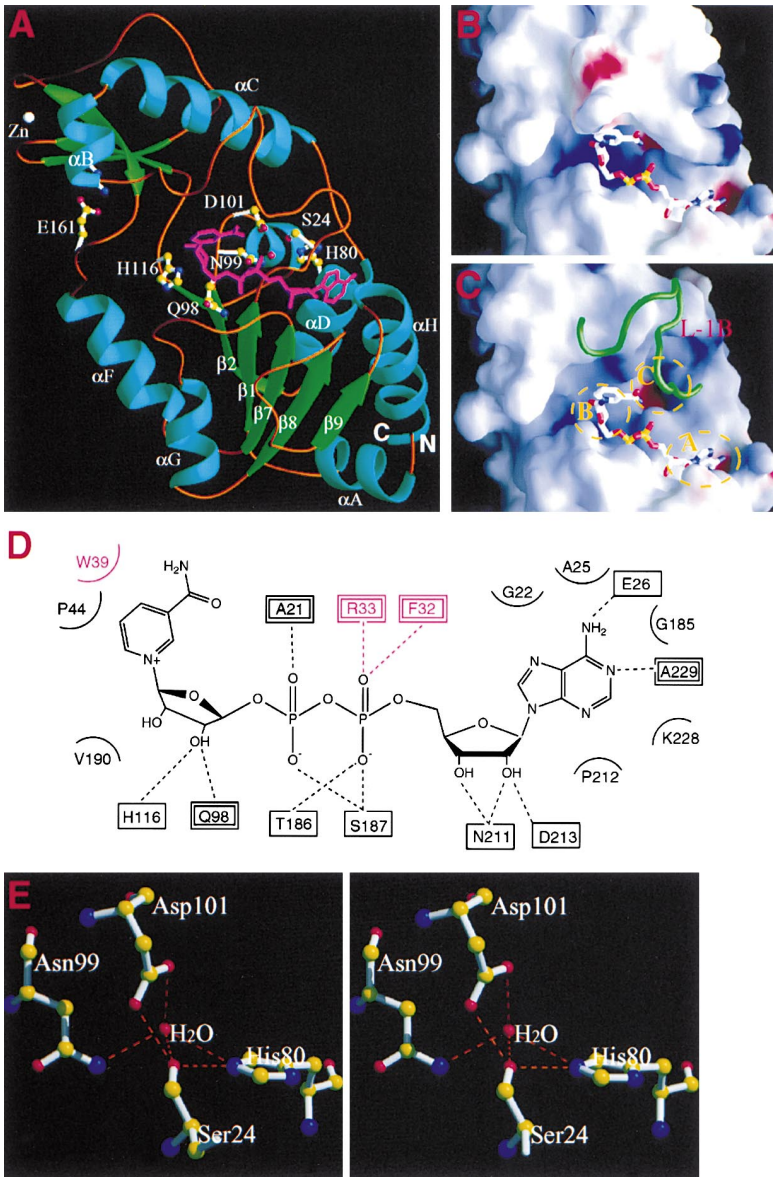

Figure 3. NAD Binding Pocket

(A) A ribbon diagram showing the NAD binding pocket in the open conformation. Key residues discussed in the text are shown in a ball-and-stick model. The NAD molecule is shown in a magenta stick model. The figure was generated with the Ribbons program (Carson, 1997).

(B) The NAD binding pocket is shown in a GRASP (Nicholls et al., 1991) surface representation. Blue and red patches indicate surface electrostatic potential distribution for positively and negatively charged residues, respectively. The NAD molecule is shown in a bond representation (red: oxygen; blue: nitrogen; white:carbon; and yellow: phosphorus).

(C) To visualize the inside of the NAD binding pocket better, a loop L-1B segment (aa 30–47) is shown as a coil (green). The rest of the structure is shown in a surface representation as in (B). Three distinct regions inside the pocket, designated A, B, and C sites are indicated and enclosed by yellow dashed lines.

(D) A schematic drawing showing direct interactions between SIR2-Af1 and NAD. Hydrogen bonds are shown in dashed lines. An arc next to the residue name indicates the amino acid is involved in van der Waals interaction with NAD. Amino acid names enclosed in a single box indicates side chain interactions while the ones enclosed in double boxes are involved in main chain interactions. Amino acids and their hydrogen bonds shown in magenta indicate additional contacts in the "closed" (orthorhombic) structure.

(E) A stereo diagram showing conserved residues and a buried water molecule at the C site. Hydrogen bonds are indicated with dashed lines.

group is in the vicinity of Phe32, Arg33, and Trp39. In the monoclinic structure, the location of the ribose group places the nicotinamide in a region next to Phe32, Arg33, and Pro44.

The C site is located deep inside the NAD binding pocket, and it is inaccessible when NAD is bound. The C site is clustered with conserved polar residues Ser24, His80, Asn99, and Asp101. These residues are all located on the "floor" and little change is noticed between the two structures. The C site is ~10 Å away from the B site where the nicotinamide ribose is situated. At the C site, Ser24 makes hydrogen bonds with His80 and Asp101 (Figure 3E). His80 is buried and interacts with Asp101 via a buried water molecule (Figure 3E). Asn99 interacts with those three residues via the same water molecule. Although the C site is not in contact with the NAD molecule in the structure, mutating the corresponding residues of Ser24 and Asn99 in yeast HST2 protein severely affected the enzymatic activity (see below).

Zinc Binding Site

Most SIR2 family members contain a Cys-X-X-Cys-$(X)_{15–20}$-Cys-X-X-Cys sequence motif in the middle of the conserved domain. This sequence motif is characteristic of certain Zn binding motifs. The cysteines are important for the function of SIR2. Replacing them with alanines abolishes the SIR2 function in *HM*, telomeric, and rDNA silencing (Sherman et al., 1999). A SIR2 mutant with all four cysteines replaced with alanines also abolishes in vitro NAD-dependent histone deacetylase activity (data not shown). No exogenous added Zn ions are needed for in vitro deacetylase and nicotinamide-NAD exchange activity. However, the zinc chelator o-phenanthroline does inhibit the enzymatic activity of HST2 at a relatively high concentration, 20 mM (data not shown). We demonstrated directly that zinc is present in recombinant SIR2-Af1 by measuring the zinc K-edge X-ray absorption and emission spectrum of SIR2-Af1 crystals (data not shown).

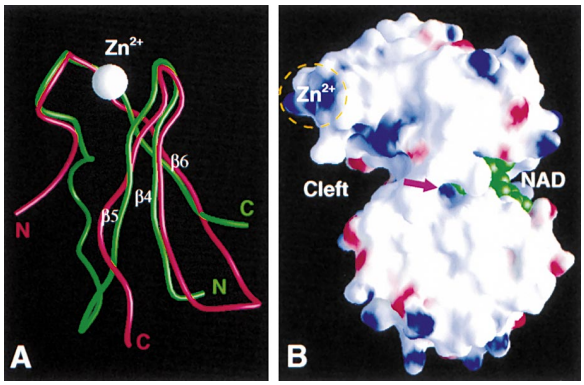

Figure 4. The SIR2-Af1 Zinc Ribbon Structure

(A) The Cα chain of the SIR2-Af1 zinc ribbon motif (Leu119-Gly160, shown in green) is superimposed with that of the zinc ribbon motif of *P. furiosus* TfIIB (Zhu et al., 1996), shown in red. The zinc ion in SIR2-Af1 is shown as a white ball. Notice that the connectivity of β strands and the chain termini positions are different in two zinc ribbons.

(B) A GRASP surface representation showing the location of the zinc ribbon in the structure. The zinc binding site is indicated with a yellow circle. A large cleft is formed between the zinc ribbon and the large domain. The cleft is proposed to be the protein substrate binding site, and it is near the putative acetyl-lysine binding channel (indicated with a magenta arrow). NAD is shown in a CPK model colored green.

In the SIR2-Af1 structure, a zinc ion is located in the small domain far away from the NAD binding pocket, excluding the possibility that it participates in the catalysis. This is in contrast with another type of protein deacetylase where Zn ions are part of the active site (Finnin et al., 1999). The zinc ion is bound between the tip of the β4-β5 turn and the loop L-56 segment proximal to β6. The zinc ion has an apparent role in holding together β4, β5, β6, and loop L-56 in the absence of extensive hydrophobic contacts. The zinc ion is replaced by a mercury ion in the orthorhombic crystal form, resulting from cocrystallization with mercury acetate for MAD phasing. No significant differences were observed between the zinc and mercury bound structures except for a segment of loop L-1B, where the difference is attributed to crystal packing interactions rather than a direct Zn binding effect. A tetrahedral coordination of the zinc ion by the sulfhydryl groups of Cys124, Cys127, Cys145, and Cys148 is observed. The three-stranded zinc binding motif is structurally homologous to the zinc ribbon motif found so far only in proteins belonging to basal transcription complexes (Qian et al., 1993; Zhu et al., 1996; Wang et al., 1998). It is interesting to note that the zinc ribbon connectivity of β strands in the present structure differs significantly from those in transcriptional factors (Figure 4A). Therefore, the structure of SIR2-Af1 provides a first example of a variant zinc ribbon motif.

The zinc-ribbon motif in SIR2-Af1 protrudes from the main body of the structure, forming an "overhang" over a large cleft between the two domains in the structure (Figure 4B). Surface residues inside the cleft are mostly hydrophilic. The cleft starts from the back side of the protein and continues to the front near the NAD binding pocket (Figure 4B). Remarkably, none of the polar residues inside the cleft is conserved, except for the conserved salt bridge between Arg153 and Glu161. The salt bridge appears to be important for maintaining a proper relative position between the two domains. These features of the cleft are consistent with it being a protein substrate binding site. Thus, the zinc ribbon motif in the SIR2 family of proteins has a structural role and it may be responsible for creating and maintaining a substrate binding site. The nonconserved residues in the cleft may be important for substrate specificity of the different deacetylases.

Structure-Function Correlation

Because of the lack of knowledge of a specific acetylated substrate for SIR2-Af1, a direct test of the structural prediction is not straightforward. Because of evolutionary conservation in sequence and enzyme activity, the structural prediction can be tested in better-characterized yeast proteins SIR2 or HST2. Guided by the structural information, we carried out mutagenesis on four invariant residues, Ser36, Gln115, His135, and Glu186, on HST2 (corresponding to Ser24, Gln98, His116, and Glu161 in SIR2-Af1; see Figure 1A) in this study. These residues were changed to alanines individually and their activities in NAD-nicotinamide exchange and deacetylation were measured. All four mutants show significantly reduced NAD-nicotinamide exchange (Figure 5A) and deacetylase (Figure 5B) activities. Two SIR2 mutants involving conserved residues His364 (Tanny et al., 1999; Imai et al., 2000) and Asn345 (Imai et al., 2000) (corresponding to SIR2-Af1 His116 and Asn99, respectively; see Figure 1A) have been previously described. Both mutants are defective in silencing and in vitro NAD-dependent histone deacetylase and the minor ADP-ribosyltransferase activities. The location of the HST2 and SIR2 mutants is shown in Figure 5C. All of the aforementioned mutants, except for Glu186 of HST2, map to the B or C sites, confirming the universality of the structural findings. Glu186 of HST2 corresponds to Glu161 of SIR2-Af1, which does not map to either the B or the C site, but is involved in the formation of the Arg153:Glu161 salt bridge (Figures 2C and 3A). Mutants that influence locus specificity of SIR2 (Cuperus et al., 2000) and a dominant-negative *sir2*^{P394L} mutation (Cockell et al., 2000) are all located away from the NAD binding pocket. Some of locus specificity mutants are indicated in Figure 5C, but some of them are in N- and C-terminal domains of SIR2 that are not conserved in the SIR2 family of proteins and thus not present in Af1. The *sir2*^{P394L} mutant cannot be seen in Figure 5C because it is on the back side of the structure as shown.

Residues located in site C are not in direct contact with the observed NAD molecule in the structure. Ser24 and Asn99 are located on the surface inside the NAD binding pocket and appear to play no roles in protein folding. The observation that enzymatic activity is severely affected by mutations of the equivalent amino acids in HST2 and SIR2 strongly suggests that conserved residues at the C site are directly involved in catalysis. His116 at site B also plays no structural role, but Gln98, also located at the B site, has a structural role in interacting with Thr186 located on loop L-7G. His116 interacts with the nicotinamide ribose of NAD in

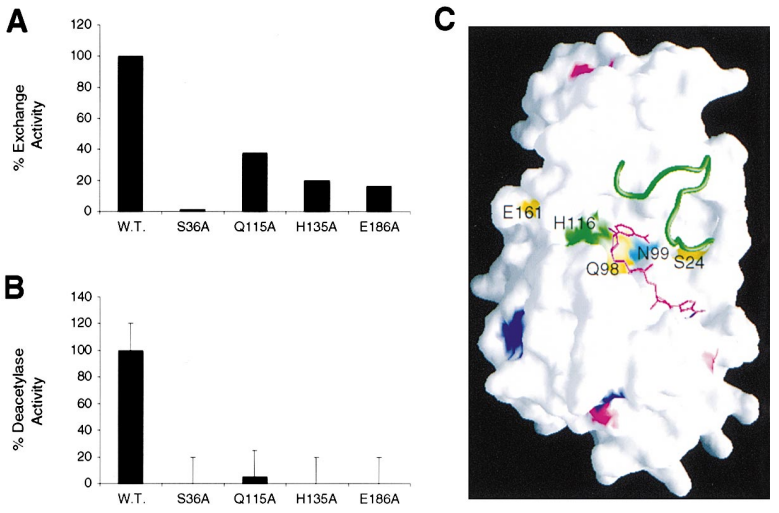

Figure 5. Nicotinamide-NAD Exchange and Deacetylase Activities of HST2 Mutants

(A) S36A, Q115A, H135A, and E186A mutants each has reduced exchange activity. Recombinant mutant proteins were assayed in an enzyme-limiting assay described in Landry et al. (2000a). Exchange was measured for 1 hr incubation by quantifying ^{14}C-labeled NAD with a phosphoimager screen using [^{14}C]nicotinamide standards. Values are expressed in percent exchange activity relative to the wild-type enzyme.

(B) S36A, Q115A, H135A, and E186A mutants each has reduced deacetylase activity. Values are expressed as percent deacetylase activity relative to the wild-type enzyme.

(C) A surface representation of the monoclinic structure showing the locations corresponding to the mutated HST2 and SIR2 residues. Positions corresponding to the mutated HST2 residues in (A) and (B) are shown in yellow or green. The green color indicates the SIR2 mutant has also been studied, and cyan indicates the residue has been studied for SIR2 only (Tanny et al., 1999; Imai et al., 2000). SIR2 locus specific mutants (Cuperus et al., 2000) are shown in blue (class I) or magenta (class II).

both structures. A direct involvement of residues at the B site in catalysis is obvious from the structure and the mutagenesis result. Glu161 of SIR2-Af1 is not at either the B or the C site, but is involved in a salt bridge that is important for maintaining a proper relative position of the zinc ribbon motif. A correct relative positioning is likely to be important for forming a protein substrate binding cleft. The lack of activity for a corresponding HST mutant suggests that even though the glutamic acid residue plays no direct role in catalysis, the structural integrity of a (potential) substrate binding site is important for the function of the SIR2 family of proteins.

Discussion

The evolutionarily conserved SIR2 family of proteins functions in diverse areas of cellular processes including transcriptional silencing, DNA repair, aging, genome stability, and cell cycle. Recent discoveries showing that these proteins are NAD-dependent protein deacetylases should greatly facilitate studies of the cellular function of this family of proteins. Understanding the structural basis of NAD-dependent protein deacetylation is crucial for mechanistic studies of this family of enzymes.

The SIR2 family of protein/histone deacetylases differs from other types of histone deacetylases in their unusual NAD requirement. Two hydrolysis steps are involved in NAD-dependent deacetylation by the SIR2 family of enzymes, namely, the cleavage of the glycosidic bond between the nicotinamide group and the ADP-ribose group of NAD and the cleavage of the C-N bond connecting the acetyl group with lysine. It has been shown recently that the SIR2-like enzymes generate a novel acetyl-ADP ribose product, 1-O-acetyl-ADP ribose, together with deacetylated lysine and free nicotinamide in a 1:1:1 molar ratio (Tanner et al., 2000; Landry et al., 2000b; Tanny and Moazed, 2001). The two catalytic steps appear to be coupled, and our structural and biochemical results provide evidence that two spatially distinct sites (sites B and C) are involved in catalysis.

Mutating conserved amino acids located in the B or C sites significantly affected enzymatic activities of yeast HST2 and SIR2. It is quite reasonable that the B site is directly involved in catalysis because it is near the observed nicotinamide ribose moiety. The involvement of the C site is not as intuitive because it is deep inside the NAD binding pocket and is not near the observed NAD molecule. Nevertheless, the unusual feature of many invariant amino acids clustered deep inside the NAD binding pocket strongly suggests that they are directly involved in catalysis. This is supported by the mutagenesis data of Ser36 of HST2 (this study) and Asn345 of SIR2 (Imai et al., 2000), both of which are located at the C site. The function of the two active sites can be distinguished by the accessibility of an acetyl-

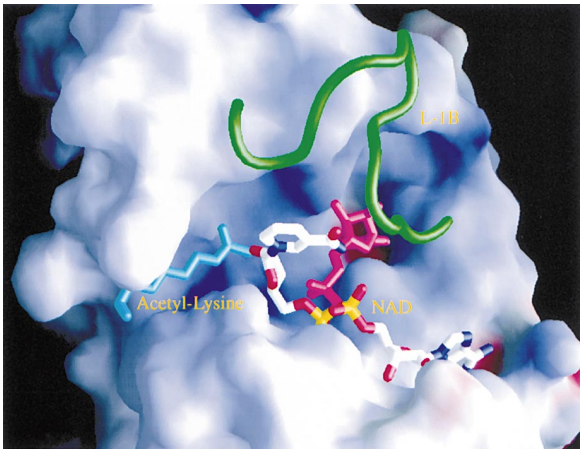

Figure 6. A Proposed Mechanism of NAD-Dependent Deacetylation

The NAD binding pocket is shown as in Figure 3C. An acetyl-lysine (shown in a cyan stick model) is docked into the proposed acetyl-lysine binding channel. A possible alternative conformation of the nicotinamide and the ribose in the presence of acetyl-lysine is shown in magenta. The alternative conformation can place the glycosidic bond next to the C site for NAD hydrolysis.

lysine. Site B can be reached by an acetyl-lysine residue with its polypeptide backbone situated outside the NAD binding pocket, while site C cannot. If one allows the polypeptide backbone to go inside the NAD binding pocket, then the binding of an acetyl-lysine at the C site and NAD in the NAD binding pocket will be mutually exclusive. These structural and biochemical considerations lead us to conclude that the B and C sites are sites for deacetylation and NAD hydrolysis, respectively.

The structure suggests a possible model for NAD-dependent protein deacetylation. In this model, the nicotinamide group is first cleaved at the C site. Although the nicotinamide group is not close to the C site in the present structures, a conformational change of NAD placing the nicotinamide group next to the C site can be modeled (Figure 6). A rotation around the ester bond between the adenine ribose and the pyrophosphate and/or the phosphodiester bonds in the pyrophosphate moiety places the nicotinamide ribose group next to the C site. Such a conformational change of NAD, likely to be induced by the binding of acetyl-lysine, is possible because the two crystal structures suggest that loop L-1B is capable of a large conformational change. Because of a general similarity of key residues in the C site with serine proteases (Figure 3E), a possible mechanism mimicking that of serine proteases can be proposed. First, the hydroxyl group of Ser24 carries out a nucleophillic attack on the glycosidic bond of NAD, cleaving the nicotinamide from NAD and forming a Ser24-ADP ribose intermediate. Unlike the situation in serine proteases, Asp101 may be protonated because Asp101 interacts with Ser24 directly. It is formally possible that Asp101, instead of Ser24, carries out the nucleophillic attack. Nevertheless, it is not preferred here because it involves a larger conformational change of NAD to reach Asp101. Cleavage of the covalent linkage of the Ser24-ADP ribose intermediate may be achieved by the attack of the water molecule, which appears to be an integral part of the C site (Figure 3E). Nicotinamide and an ADP-ribose product, possibly an oxo-carbenium ADP ribose (Tanner et al., 2000) ion, are the products of the reaction at the C site. It is worth noting that, because the C site is deep inside, the nicotinamide is likely to be trapped inside the enzyme until the ADP-ribose product is released. It appears certainly the case when loop L-1B is in the closed conformation. Nevertheless, it is possible that nicotinamide may diffuse in or out the NAD binding pocket when the loop is in the open conformation or when it undergoes further conformational changes. Our structural and biochemical data suggest that deacetylation takes place at the B site. The ADP-ribose product produced in the first reaction at the C site can return to the initial position at the B site. A direct involvement of the oxo-carbenium ion in deacetylation is likely. A plausible model has been proposed (Tanner et al., 2000), in which the acyl oxygen of acetyl-lysine condenses with the oxo-carbenium cation directly and the intermediate then collapses to produce 1-O-acetyl-ADP ribose and deacetylated lysine. A direct participation of the oxo-carbenium ion in deacetylation is supported by the structure, as the B site lacks catalytic base or acid residues. An ordered water molecule coordinated by His116 and Pro192 can carry out the nucleophillic attack in the proposed model.

In summary, the crystal structure of SIR2-Af1 supports a sequential, coupled, two step mechanism in NAD-dependent deacetylation. First, the glycosidic bond between nicotinamide and ADP-ribose in NAD is cleaved at the C site of the enzyme with acetyl-lysine as a cofactor, and nicotinamide and an ADP ribose oxo-carbenium ion as reaction products. Second, the oxo-carbenium ion together with the protein form an active deacetylase at the B site. In addition to providing mechanistic insights into the enzymatic function, the structure also provide insights into substrate binding (Figure 4B) and sites of protein-protein interactions that might affect locus specificity of the SIR2 family of proteins (Figure 5C). Although determinants of substrate selectivity or locus specificity cannot be attributed to isolated domains or clustered amino acids, the structure provides a framework for further structure and function studies of the SIR2 family of protein/histone deacetylases.

Experimental Procedures

Protein Preparation and Enzymatic Assays

Genomic DNA of *A. fulgidus* was purchased from American Type Culture Collection (ATCC). A PCR fragment of the coding sequence of SIR2-Af1 was cloned into a pQE30 vector (Qiagen) between the BamHI and HindIII sites. The resultant plasmid expresses poly-histidine tagged SIR2-Af1 in XL1Blue *E. coli* cells. Poly-histidine tagged SIR2-Af1 was purified by Ni-NTA (Qiagen), Mono-S, and Superdex-200 (Pharmacia) column chromatographies. HST2 mutants were made with a site-directed mutagenesis kit (Stratagene) according to the manufacturer's instructions. Mutant proteins were prepared as described in Landry et al. (2000a).

NAD-nicotinamide exchange assay of SIR2-Af1 was performed according to Landry et al. (2000a) at 50°C for 1.5 hr in a buffer containing 50 mM acetate (pH 5.0), 5 mM sodium phosphate, and 0.5 M NaCl. The reaction was carried out in a 20 μl volume with 0.5 μg of enzyme, 0.5 mM NAD, 0.2 mg/ml acetylated BSA, and 0.1 mM [^{14}C]nicotinamide. The exchange assay with HST2 was performed analogously at 30°C. Deacetylase activity of SIR2-Af1 was measured by detecting the release of [^{3}H]acetate from [^{3}H]acetylated BSA.

BSA was acetylated using [^{3}H]acetate and a carbodiimide coupling reagent. Reactions were performed in 140 μl using 7 mg/ml BSA (Sigma), 100 mM MES (pH 5.0), 250 μCi [^{3}H]acetate (ICN) and 2.2 mg/ml EDC (Pierce). Reactions were incubated at room temperature for 2 hr. [^{3}H]acetylated BSA was desalted in 50 μl aliquots using G-50 Micro Spin columns. One milligram of the desalted [^{3}H]acetylated BSA was acid precipitated in 500 μl ice cold 20% TCA for 20 min. Precipitated [^{3}H]acetylated BSA was recovered by centrifugation, and the pellet was washed three times with 500 μl of ice cold acetone. The pellet was air dried and redissolved in 100 μl deionized water.

SIR2-Af1 deacetylation assays were performed at 50°C in 200 μl using 50 mM citrate (pH 4.5), 5 mM P_2O_7, 0.5 mM DTT, 500 mM NaCl, 500 μM NAD, 50 μg [^{3}H]acetylated BSA, and 2 μg SIR2-Af1. HST2 deacetylation reactions were performed similarly at 30°C in a glycine buffer (pH 9.0) and with 1.6 μg HST2. Both reactions were carried out for 3 hr, and then the reactions were quenched by adding 30 μl 1N NaOH and incubated at room temperature for 20 min. After quenching, the reactions were reacidified by adding 60 μl of 1 N HCl, 0.4 M acetic acid and extracted with 1 ml water-saturated ethyl acetate. Seven hundred microliters of the organic phase was removed and added to 3 ml of scintillation fluid. Samples were counted in a scintillation counter to determine the amount of ^{3}H released from the acetylated BSA.

Crystallization and Structure Determination

Purified protein was concentrated to ~20 mg/ml in a buffer containing 5 mM Tris (pH 8.0), 200 mM NaCl, 0.1% β-mercaptomethanol, and 1 mM EDTA. Concentrated SIR2-Af1 protein was mixed with NAD at a final concentration of 6 mM, and the mixture was incubated

on ice for 30 min to allow complex formation. SIR2-Af1/NAD complex crystals were grown by the hanging-drop vapor diffusion method at 16°C. The monoclinic crystals were grown in a condition containing 100 mM MES (pH 6.0), and 12% PEG-10K. The orthorhombic crystals were grown in the same condition supplemented with 1 mM cetyltrimethylammonium bromide (CTAB). Mercury substituted orthorhombic crystals were grown in the presence of 1 mM mercury acetate.

X-ray diffraction data were collected at beamlines X12C and X26C of National Synchrotron Light Source (NSLS) at Brookhaven National Laboratory (BNL). Data were collected with crystals flash-cooled to 95°K and processed using DENZO and SCALEPACK programs (Otwinowski and Minor, 1997). The orthorhombic structure was solved first using the MAD method. The orthorhombic crystals are in the $C222_1$ space group with a = 57.83 Å, b = 122.17 Å, and c = 154.48 Å. There are two protein/NAD complexes per asymmetric unit. A mercurial derivative was used for MAD phasing (mercurial derivatives diffracted better than the unsoaked orthorhombic crystals). PHASES program (Furey and Swaminathan, 1997) was used for phasing with three-wavelength (λ_1 = 1.01089 Å, λ_2 = 1.00842 Å, and λ_3 = 1.00393 Å) mercurial MAD data at 2.8 Å resolution. Solvent flattening and 2-fold noncrystallographic symmetry averaging were used to improve the accuracy of phases. Graphic program O (Jones et al., 1991) was used for model building, and CNS (Brünger et al., 1998) was used for refinement. The model was refined against a 2.4 Å mercurial derivative data set collected at a 1.1 Å (λ_0) wavelength. During the refinement, R_{free} was monitored by using 8% of the data. The final model has 88% of the protein main chain ϕ/ψ angles in the most favored region and none in the disallowed region of the Ramachandran plot, calculated using PROCHECK (Laskowski et al., 1993).

The monoclinic crystal has a C2 spacegroup with cell dimensions of a = 65.41 Å, b = 94.54 Å, c = 93.78 Å, and β = 95.29°. The monoclinic structure was solved by molecular replacement using the CNS program suite and diffraction data in the 15.0–4.0 Å resolution range. The initial R factor for the molecular replacement solution was 42% for all the data lower than or equal to 3.0 Å resolution. The final model includes an eleven amino acid (out of thirteen possible) poly-histidine tag in one of the protein molecules. The model was refined to 2.1 Å resolution (8% data was set aside and used for calculating R_{free}), and 89% of the main chain ϕ/ψ angles are in the most favored region, and none in the disallowed region of the Ramachandran plot.

Acknowledgments

We thank Dieter Schneider, Anand Saxena, and Robert M. Sweet for help at National Synchrotron Light Source, Brookhaven National Laboratory, and Troy Messick for comments on the manuscript. J. M. was supported by a Cold Spring Harbor Laboratory Association fellowship. The work was supported in part by National Institutes of Health Grant GM55641 (R. S.) and by the W. M. Keck foundation (R. M. X.).

Received December 27, 2000; revised March 9, 2001.

References

Afshar, G., and Murnane, J.P. (1999). Characterization of a human gene with sequence homology to Saccharomyces cerevisiae SIR2. Gene *234*, 161–168.

Allshire, R.C. (1996). Transcriptional silencing in fission yeast: a manifestation of higher order chromosome structure and functions. In Epigenetic Mechanisms of Gene Regulation, V.E. Russo, R.A. Martienssen, and A. Riggs, eds. (Cold Spring Harbor, NY: Cold Spring Harbor Laboratory Press), pp. 443–466.

Aparicio, O.M., Billington, B.L., and Gottschling, D.E. (1991). Modifiers of position effect are shared between telomeric and silent mating-type loci in S. cerevisiae. Cell *66*, 1279–1287.

Brachmann, C.B., Sherman, J.M., Devine, S.E., Cameron, E.E., Pillus, L., and Boeke, J.D. (1995). The SIR2 gene family, conserved from bacteria to humans, functions in silencing, cell cycle progression, and chromosome stability. Genes Dev. *9*, 2888–2902.

Braunstein, M., Rose, A.B., Holmes, S.G., Allis, C.D., and Broach, J.R. (1993). Transcriptional silencing in yeast is associated with reduced nucleosome acetylation. Genes Dev. *7*, 592–604.

Bryk, M., Banerjee, M., Murphy, M., Knudsen, K.E., Garfinkel, D.J., and Curcio, M.J. (1997). Transcriptional silencing of Ty1 elements in the RDN1 locus of yeast. Genes Dev. *11*, 255–269.

Brünger, A.T., Adams, P.D., Clore, G.M., DeLano, W.L., Gros, P., Grosse-Kunstleve, R.W., Jiang, J.S., Kuszewski, J., Nilges, M., Pannu, N.S., et al. (1998). Crystallography and NMR system: A new software system for macromolecular structure determination. Acta Crystallogr. D *54*, 905–921.

Carson, M. (1997). Ribbons. Method Enzymol. *277*, 493–505.

Cockell, M.M., Perrod, S., and Gasser, S.M. (2000). Analysis of SIR2 domains required for rDNA and telomeric silencing in Saccharomyces cerevisiae. Genetics *154*, 1069–1083.

Cuperus, G., Shafaatian, R., and Shore, D. (2000). Locus specificity determinants in the multifunctional yeast silencing protein Sir2. EMBO J. *19*, 2641–2651.

Finnin, M.S., Donigian, J.R., Cohen, A., Richon, V.M., Rifkind, R.A., Marks, P.A., Breslow, R., and Pavletich, N.P. (1999). Structures of a histone deacetylase homologue bound to the TSA and SAHA inhibitors. Nature *401*, 188–193.

Fritze, C.E., Verschueren, K., Strich, R., and Esposito, R.E. (1997). Direct evidence for SIR2 modulation of chromatin structure in yeast rDNA. EMBO J. *16*, 6495–6509.

Frye, R.A. (1999). Characterization of five human cDNAs with homology to the yeast SIR2 gene: Sir2-like proteins (sirtuins) metabolize NAD and may have protein ADP-ribosyltransferase activity. Biochem. Biophys. Res. Commun. *260*, 273–279.

Furey, W., and Swaminathan, S. (1997). PHASES-95: a program package for the processing and analysis of diffraction data from macromolecules. Methods Enzymol. *277*, 590–620.

Gartenberg, M.R. (2000). The Sir proteins of Saccharomyces cerevisiae: mediators of transcriptional silencing and much more. Curr. Opin. Microbiol. *3*, 132–137.

Gottschling, D.E., Aparicio, O.M., Billington, B.L., and Zakian, V.A. (1990). Position effect at S. cerevisiae telomeres: Reversible repression of Pol II transcription. Cell *63*, 751–762.

Gottschling, D.E. (2000). Gene silencing: two faces of SIR2. Curr. Biol. *10*, R708–711.

Guarente, L. (2000). Sir2 links chromatin silencing, metabolism, and aging. Genes Dev. *14*, 1021–1026.

Hecht, A., Laroche, T., Strahl-Bolsinger, S., Gasser, S.M., and Grunstein, M. (1995). Histone H3 and H4 N-termini interact with SIR3 and SIR4 proteins: a molecular model for theformation of heterochromatin in yeast. Cell *80*, 583–592.

Hecht, A., Strahl-Bolsinger, S., and Grunstein, M. (1996). Spreading of transcriptional repressor SIR3 from telomeric heterochromatin. Nature *383*, 92–96.

Holm, L., and Sander, C. (1996). Alignment of three-dimensional protein structures: network server for database searching. Methods Enzymol. *266*, 653–662.

Imai, S., Armstrong, C.M., Kaeberlein, M., and Guarente, L. (2000). Transcriptional silencing and longevity protein Sir2 is an NAD-dependent histone deacetylase. Nature *403*, 795–800.

Johnson, L.M., Kayne, P.S., Kahn, E.S., and Grunstein, M. (1990). Genetic evidence for an interaction between SIR3 and histone H4 in the repression of the silent mating loci in Saccharomyces cerevisiae. Proc. Natl. Acad. Sci. USA *87*, 6286–6290.

Jones, T.A., Zou, J.Y., Cowan, S.W., and Kjeldgard, M. (1991). Improved methods for building protein models in electron density maps and the location of errors in these models. Acta Crystallogr. A *47*, 110–119.

Kraulis, P.J. (1991). MOLSCRIPT: a program to produce both detailed and schematic plots of proteins. J. Appl. Crystsllogr. *24*, 946–956.

Laskowski, R.A., MacArthur, M.W., Moss, D.S., and Thornton, J.M. (1993). PROCHECK: a program to check the stereochemical quality of protein structures. J. Appl. Crystsllogr. *26*, 283–291.

Landry, J., Sutton, A., Tafrov, S.T., Heller, R.C., Stebbins, J., Pillus, L., and Sternglanz, R. (2000a). The silencing protein SIR2 and its homologs are NAD-dependent protein deacetylases. Proc. Natl. Acad. Sci. USA *97*, 5807–5811.

Landry, J., Slama, J.T., and Sternglanz, R. (2000b). Role of NAD(+) in the deacetylase activity of the SIR2-like proteins. Biochem. Biophys. Res. Commun. *278*, 685–690.

Laurenson, P., and Rine, J. (1992). Silencers, silencing, and heritable transcriptional states. Microbiol. Rev. *56*, 543–560.

Lin, S.J., Defossez, P.A., and Guarente, L. (2000). Requirement of NAD and SIR2 for life-span extension by calorie restriction in Saccharomyces cerevisiae. Science *289*, 2126–2128.

Loo, S., and Rine, J. (1995). Silencing and heritable domains of gene expression. Annu. Rev. Cell. Dev. Biol. *11*, 519–548.

Lyon, M.F. (1999). X-chromosome inactivation. Curr. Biol. *9*, R235–237.

Merritt, E.A., and Bacon, D.J. (1997). Raster 3D: photorealistic molecular graphics. Methods Enzymol. *277*, 505–524.

Moretti, P., Freeman, K., Coodly, L., and Shore, D. (1994). Evidence that a complex of SIR proteins interacts with the silencer and telomere-binding protein RAP1. Genes Dev. *8*, 2257–2269.

Moazed, D., Kistler, A., Axelrod, A., Rine, J., and Johnson, A.D. (1997). Silent information regulator protein complexes in Saccharomyces cerevisiae: a SIR2/SIR4 complex and evidence for a regulatory domain in SIR4 that inhibits its interaction with SIR3. Proc. Natl. Acad. Sci. USA *94*, 2186–2191.

Nicholls, A., Sharp, K.A., and Honig, B. (1991). Protein folding and association: insights from the interfacial and thermodynamic properties of hydrocarbons. Proteins *11*, 281–296.

Otwinowski, Z., and Minor, W. (1997). Processing of X-ray diffraction data collected in oscillation mode. Methods Enzymol. *276*, 307–326.

Prasad, G.S., Sridhar, V., Yamaguchi, M., Hatefi, Y., and Stout, C.D. (1999). Crystal structure of transhydrogenase domain III at 1.2 Å resolution. Nat. Struct. Biol. *6*, 1126–1131.

Qian, X., Gozani, S.N., Yoon, H., Jeon, C.J., Agarwal, K., and Weiss, M.A. (1993). Novel zinc finger motif in the basal transcriptional machinery: three-dimensional NMR studies of the nucleic acid binding domain of transcriptional elongation factor TFIIS. Biochemistry *32*, 9944–9959.

Rine, J., and Herskowitz, I. (1987). Four genes responsible for a position effect on expression from HML and HMR in Saccharomyces cerevisiae. Genetics *116*, 9–22.

Rossmann, M.G., Liljas, A., Brändén, C.I., and Banaszak, L.J. (1975). Evolutionary and structural relationships among dehydrogenases. In The Enzymes, 3rd edition., P.D. Boyer, ed. (New York: Academic Press) Vol. XI., pp. 61–102.

Sherman, J.M., Stone, E.M., Freeman-Cook, L.L., Brachmann, C.B., Boeke, J.D., and Pillus, L. (1999). The conserved core of a human SIR2 homologue functions in yeast silencing. Mol. Biol. Cell. *10*, 3045–3059.

Shou, W., Seol, J.H., Shevchenko, A., Baskerville, C., Moazed, D., Chen, Z.W., Jang, J., Shevchenko, A., Charbonneau, H., and Deshaies, R.J. (1999). Exit from mitosis is triggered by Tem1-dependent release of the protein phosphatase Cdc14 from nucleolar RENT complex. Cell *97*, 233–244.

Smith, J.S., and Boeke, J.D. (1997). An unusual form of transcriptional silencing in yeast ribosomal DNA. Genes Dev. *11*, 241–254.

Smith, J.S., and Boeke, J.D. (1997). An unusual form of transcriptional silencing in yeast ribosomal DNA. Genes Dev. *11*, 241–254.

Smith, J.S., Brachmann, C.B., Celic, I., Kenna, M.A., Muhammad, S., Starai, V.J., Avalos, J.L., Escalante-Semerena, J.C., Grubmeyer, C., Wolberger, C., and Boeke, J.D. (2000). A phylogenetically conserved NAD+-dependent protein deacetylase activity in the Sir2 protein family. Proc. Natl. Acad. Sci. USA *97*, 6658–6663.

Straight, A.F., Shou, W., Dowd, G.J., Turck, C.W., Deshaies, R.J., Johnson, A.D., and Moazed, D. (1999). Net1, a Sir2-associated nucleolar protein required for rDNA silencing and nucleolar integrity. Cell *97*, 245–256.

Strahl-Bolsinger, S., Hecht, A., Luo, K., and Grunstein, M. (1997). SIR2 and SIR4 interactions differ in core and extended telomeric heterochromatin in yeast. Genes Dev. *11*, 83–93.

Tanner, K.G., Landry, J., Sternglanz, R., and Denu, J.M. (2000). Silent information regulator 2 family of NAD-dependent histone/protein deacetylases generates a unique product, 1-O-acetyl-ADP-ribose. Proc. Natl. Acad. Sci. USA *97*, 14178–14182.

Tanny, J.C., Dowd, G.J., Huang, J., Hilz, H., and Moazed, D. (1999). An enzymatic activity in the yeast Sir2 protein that is essential for gene silencing. Cell *99*, 735–745.

Tanny, J.C., and Moazed, D. (2001). Coupling of histone deacetylation to NAD breakdown by the yeast silencing protein Sir2: Evidence for acetyl transfer from substrate to an NAD breakdown product. Proc. Natl. Acad. Sci. USA *98*, 415–420.

Tsang, A.W., and Escalante-Semerena, J.C. (1998). CobB, a new member of the SIR2 family of eucaryotic regulatory proteins, is required to compensate for the lack of nicotinate mononucleotide:5,6-dimethylbenzimidazole phosphoribosyltransferase activity in cobT mutants during cobalamin biosynthesis in Salmonella typhimurium LT2. J. Biol. Chem. *273*, 31788–31794.

Tsukamoto, Y., Kato, J., and Ikeda, H. (1997). Silencing factors participate in DNA repair and recombination in Saccharomyces cerevisiae. Nature *388*, 900–903.

Wang, B., Jones, D.N., Kaine, B.P., and Weiss, M.A. (1998). High-resolution structure of an archaeal zinc ribbon defines a general architectural motif in eukaryotic RNA polymerases. Structure *6*, 555–569.

Weiler, K.S., and Wakimoto, B.T. (1995). Heterochromatin and gene expression in Drosophila. Annu. Rev. Genet. *29*, 577–605.

Zhu, W., Zeng, Q., Colangelo, C.M., Lewis, M., Summers, M.F., and Scott, R.A. (1996). The N-terminal domain of TFIIB from Pyrococcus furiosus forms a zinc ribbon. Nat. Struct. Biol. *3*, 122–124.

Protein Data Bank ID Code

Atomic coordinates of the Sir2 Homolog–NAD complex reported in this paper have been deposited in the Protein Data Bank under ID code 1ICI.